

<https://doi.org/10.1038/s43246-024-00509-0>

# The collective photothermal effect of silver nanoparticles probed by a microbolometer

Check for updates

Hanliang Zhu<sup>1,3</sup>, Evelína Gablech<sup>2,3</sup>, Imrich Gablech<sup>2</sup>✉ & Pavel Neuzil<sup>1</sup>✉

Nanoparticles have become a significant area of research, offering properties that bridge the gap between bulk materials and atomic structures. Silver nanoparticles (AgNPs), specifically, have shown promise due to their plasmonic properties. Despite extensive studies, capturing the photon-to-heat conversion efficiency of individual nanoparticles has been challenging. Here, we present an approach to determine these properties using an ultra-sensitive bolometer with a power resolution of  $\approx 26$  pW. Our investigations reveal that a single AgNP can dissipate power with a magnitude between  $\approx 101.3$  fW and  $\approx 205.3$  fW, an observation that underscores the potential of these particles for efficient energy conversion. This finding enhances the understanding of AgNPs' behavior and pushes the field of nanoparticle plasmon physics forward. Therefore, the refined use of such nanoparticles could bring advancements across a range of applications, from high-resolution imaging and advanced spectroscopy to environmental surveillance and innovative medical treatments.

Plasmonic nanoparticles, with their distinctive optical properties, have garnered significant attention in many scientific domains<sup>1,2</sup>, from biomedicine to environmental science<sup>3,4</sup>. Among all nanoparticles, silver nanoparticles (AgNPs) attract attention due to their pronounced localized surface plasmon resonance (LSPR) capabilities<sup>5,6</sup>. This LSPR phenomenon, a collective oscillation of conduction electrons stimulated by incoming light, grants AgNPs the remarkable capability to amplify and confine electromagnetic fields at the nanoscale<sup>7</sup>, rendering them applicable to diverse sectors<sup>8</sup>. Furthermore, these nanoparticles can transform absorbed light energy into heat through the photothermal effect (PTE)<sup>9,10</sup>. This feature has been instrumental in various domains, including cancer treatment, where light-induced heating targets and eradicates cancer cells<sup>11,12</sup>.

Bolometers, known for their ultra-sensitive heat detection capable of sensing heat from a human even from considerable distances<sup>13–15</sup>, operate by converting thermal variations into changes in electrical resistance. Their versatile applications span infrared astronomy<sup>13</sup>, thermal imaging<sup>16</sup>, materials characterization<sup>17</sup>, preventive maintenance<sup>18</sup>, and, in recent years, thermal imaging of newly constructed homes<sup>19</sup>.

Introducing AgNPs to bolometer membrane surfaces seems promising, given bolometers' power sensitivity and resolution. Unfortunately,

bolometers cannot measure individually local events on their membrane, only a global membrane dynamic and static temperature response. The deposition process of AgNPs is influenced by electrostatic adsorption between the bolometer membrane and the AgNPs. This adsorption is subject to the surface charges of both entities, which can be modulated by the environmental pH value. As pH levels shift, the activity of hydroxonium ions ( $\text{H}_3\text{O}^+$ ) changes, potentially impacting the surface charge through protonation or deprotonation events<sup>20</sup>. Harnessing the heat-conversion capability of AgNPs could further optimize bolometer power efficiency.

In this study, we provide a comprehensive examination of the power dissipated at the bolometer surface after illumination due to the presence of attached AgNPs. Investigation into resulting changes in the bolometers' thermal and spectral behaviors enabled us to estimate the power dissipated by a single AgNP. Furthermore, we explored the influence of pH values on the deposition process of AgNPs on bolometer surfaces. Evaluations considering the distribution and size effects of AgNPs on bolometer response are also shared. Our findings elucidate the potential of AgNPs to probe plasmonic properties and enhance bolometer efficiency. We anticipate that our insights will inspire further exploration in this innovative field of nanotechnology.

<sup>1</sup>Northwestern Polytechnical University, Ministry of Education Key Laboratory of Micro/Nano Systems for Aerospace, Department of Microsystem Engineering, School of Mechanical Engineering, 127 West Youyi Road, 710072 Xi'an, Shaanxi, P. R. China. <sup>2</sup>Department of Microelectronics, Faculty of Electrical Engineering and Communication, Brno University of Technology, Technická 3058/10, 616 00, Brno, Czech Republic. <sup>3</sup>These authors contributed equally: Hanliang Zhu, Evelína Gablech. ✉e-mail: [imrich.gablech@vutbr.cz](mailto:imrich.gablech@vutbr.cz); [pavel.neuzil@nwpu.edu.cn](mailto:pavel.neuzil@nwpu.edu.cn)

## Results and discussion

### Design and characterization of the high-sensitive bolometer

The bolometer employed in this study builds on previous designs<sup>21,22</sup>, refined using the Nanolithography Toolbox<sup>23,24</sup> for layout generation. Our bolometer membrane, with a designed sensitive area of  $(25 \times 25) \mu\text{m}^2$ , was anchored by two  $\text{SiO}_2$  legs to improve the thermal insulation. The sensing element of the bolometer was in a resistance temperature detector (RTD) made from Ti in the suspended area. The bolometer membrane was ultra-sensitive to radiation power; here, it functioned as a temperature sensor to study the PTE of AgNPs (Fig. 1a). We fabricated the bolometers through micromachining technology and modified AgNPs on their surface using the electrostatic deposition method (Fig. 1b). Each chip featured 48 individual bolometers at the center, and each bolometer had its extension leads and pads for further wire bonding (Fig. 1c and d). Our final bolometer legs each had measured dimensions of  $\approx 1.2 \mu\text{m}$  for width,  $\approx 0.424 \mu\text{m}$  for thickness, and  $\approx 62 \mu\text{m}$  for length for excellent thermal isolation.

The device, comprising two Si chips, each housing 48 bolometers, having one device with and the other without the AgNPs paired together, was positioned in a vacuum chamber. Each bolometer had an independent electrical connection. Two bolometers, one with and one without AgNPs and both with a resistance ( $R$ ) of  $\approx 10.86 \text{ k}\Omega$ <sup>25</sup>, were incorporated into an AC-powered Wheatstone bridge under a voltage bias ( $V_B$ ) in differential mode. The differential voltage ( $\Delta V = V_1 - V_2$ ) derived from the bridge outputs was further processed by a lock-in amplifier, with the result ( $\Delta V_L$ ) being recorded by an oscilloscope (Fig. 2a)<sup>26</sup>. The bolometers were exposed to light from an Xe lamp via a grating monochromator and liquid core optical fiber. The vacuum chamber was thermally shielded and maintained an internal pressure of  $\approx 12 \text{ mPa}$ , reducing the bolometer membrane's temperature fluctuations.

The PTE of AgNPs was evaluated by monitoring the dissipated power by bolometer when shining light on the AgNPs deposited membrane. We used an Xe lamp providing light with a spectrum wavelength from 260 to 1000 nm. This light source was connected via liquid core optical fiber to a grating monochromator to select the desired wavelength to illuminate the bolometer in the vacuum chamber (Fig. 2b). During the PTE measurement,

the scanning step duration for each photon wavelength ( $\lambda$ ) was set to 10 s, with an additional  $\approx 1 \text{ s}$  needed for changing values and stabilization of the monochromator. A MATLAB script was used to compute the average value for each wavelength, with data processing undertaken using the *Origin* software (Fig. 2c).

The temperature coefficient of resistance TCR ( $\alpha$ ) of the bolometer was characterized using the method mentioned in the previous section, and the results of  $R$  as a function of temperature ( $T$ ) were plotted. We adopted a linear curve fitting as the resistance ( $R$ ) varied with temperature ( $\Delta T$ ) can be approximated this way:

$$R = R_0(1 + \alpha \cdot \Delta T), \quad (1)$$

where  $R_0$  is the sensor's resistance at  $0^\circ\text{C}$ , and  $\alpha$  represents the TCR. The calculated values,  $R_0$  and  $\alpha$ , of the tested bolometer were  $(9.98 \pm 1.14 \times 10^{-3}) \text{ k}\Omega$  and  $(0.27 \pm 7.63 \times 10^{-4}) \% \text{ K}^{-1}$ , respectively, both with (mean value  $\pm$  fitting error) (Fig. S1 in Supplementary section 1). We then formed the Wheatstone bridge consisting of a single bolometer and three fixed resistors and powered it with  $V_B$  set to 50 mV, resulting in a  $P_j$  of  $\approx 58.6 \text{ nW}$ , per Eq. (2) in the "Methods" section, and a bolometer temperature rise of  $\approx 1.47^\circ\text{C}$ , per Eq. (3) in the "Methods" section. The self-heating method facilitated the measurement of the bolometer's thermal parameters using short  $V_B$  pulses with variable  $V_{DC}$  bias<sup>27</sup> (Fig. S2a, b in Supplementary Section 2). Measurements from three bolometer sets revealed the following both thermal capacitance ( $H$ ) and conductance ( $G$ ), as well as the time constant ( $\tau$ ) as  $\approx 0.84 \text{ nJ K}^{-1}$ ,  $\approx 45.95 \text{ nW K}^{-1}$ , and  $\tau \approx 18.32 \text{ ms}$ , respectively (Fig. S2c in Supplementary Section 2). All measured thermal parameters of the different bolometers are listed in Table 1.

The resolution of the bolometer was influenced by two key aspects: thermal isolation evaluated by the  $G$  magnitude and the temperature noise of the system. The bolometer used was well isolated by the "L" shaped legs, obtaining a  $G$  value of  $\approx 45.95 \text{ nW K}^{-1}$  in a vacuum test chamber. Thus, the resolution of our bolometer depended on the temperature noise, including electrical noise in the test circuit and heat fluctuation in the test

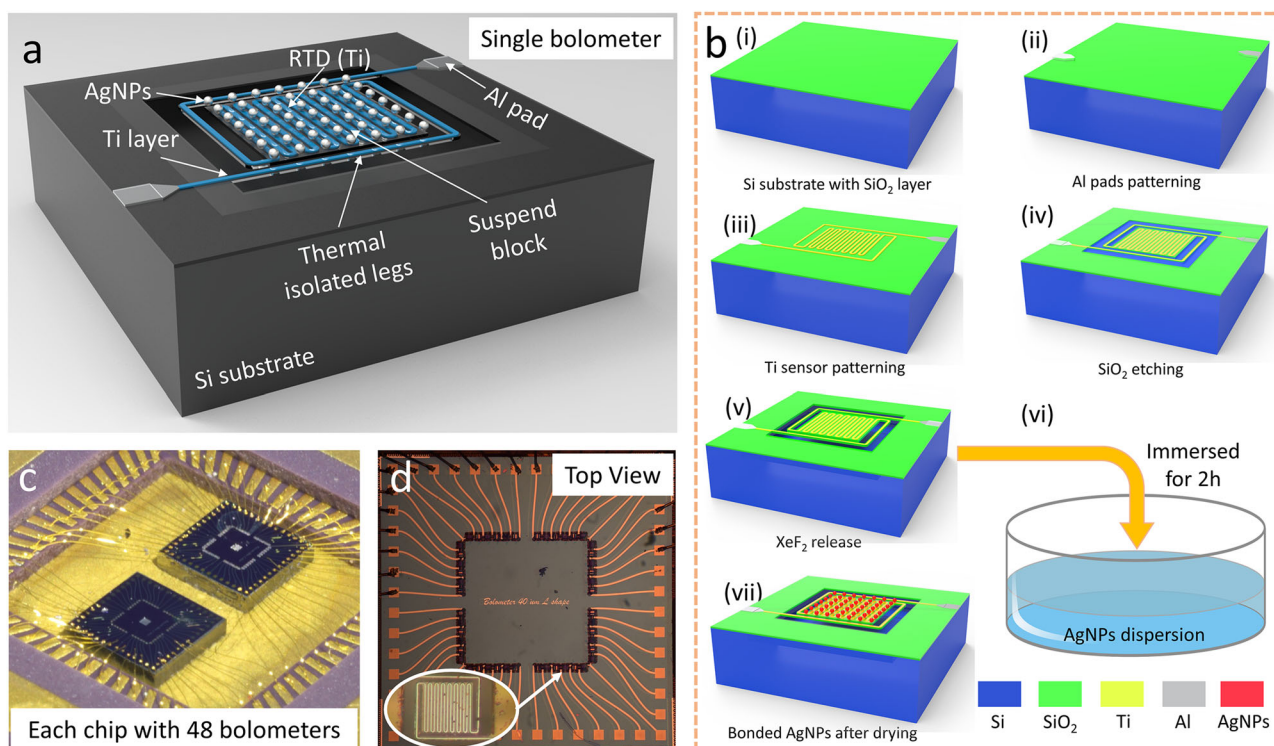


**Fig. 1 | Schematic of the bolometer design and its fabrication.** **a** Schematic of the single bolometer structure with silver nanoparticles (AgNPs). **b** Fabrication process flow of the bolometer device and AgNPs deposition. **c** Photograph of two Si chips, each with 48 individual bolometers and **d** its top view.

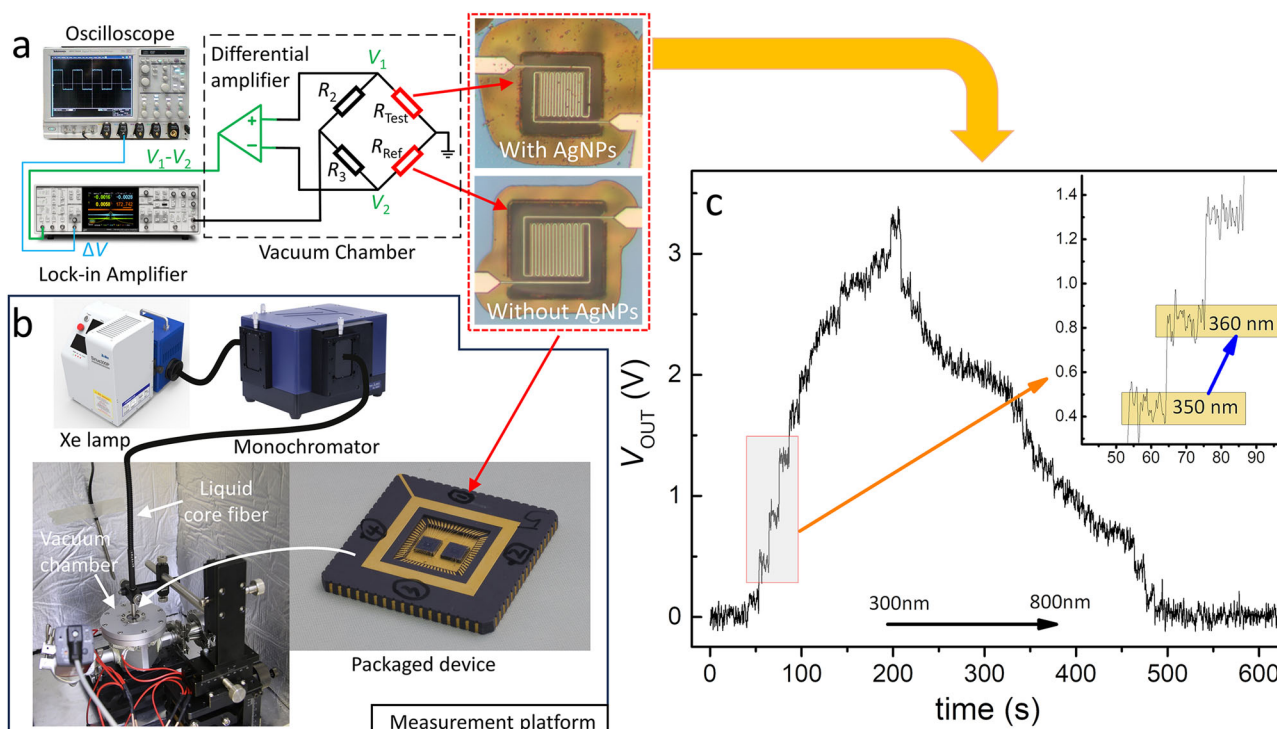


**Fig. 2 | Measurement setup using a bolometer for heat detection.** **a** Reference and testing bolometer was connected to a Wheatstone bridge with its outputs processed by a differential amplifier ( $V_1 - V_2$ ) and subsequently by a lock-in amplifier with its output ( $\Delta V_L$ ) recorded by an oscilloscope. **b** Two Si chips with bolometers, one with and one without silver nanoparticles (AgNPs), were placed into a vacuum chamber,

and the whole chamber was located in a temperature-controlled thermally shielded box. Light projected onto the bolometers originated from an Xe lamp, with a particular wavelength selected by a monochromator and delivered via a liquid core fiber. **c** Measurement output demonstrated an observed response to monochromatic light across various wavelengths.

environment. The temperature stability of the thermal isolation box was characterized using a thermometer with a resolution of  $\approx 1$  mK, which showed a fluctuation of  $\approx 0.3$  K at  $\approx 296.15$  K ( $\approx 23$  °C) throughout  $\approx 2.8$  h. This fluctuation of the environment was further decreased by the employment of the vacuum chamber, thus lowering the temperature noise. We measured the temperature noise with settings adjusted to  $V_B$ , lock-in amplifier gain factor ( $S$ ), and differential amplifier gain factor ( $B$ ) values of 50, 1 mV, and 10,000, respectively, and the  $T_T$  valve acquired as  $\approx 3.41$  kV K $^{-1}$ , per Eq. (5) in the “Methods” section. The system noise was captured and calculated at 1.381 V, obtaining the temperature noise and resolution of  $\approx 404.7$   $\mu$ K and  $\approx 26$  pW, respectively (Fig. S2d in Supplementary Section 2). Maintaining a consistent temperature is essential for accurate measurements, especially when assessing minute changes that can significantly impact readings.

The power sensitivity of the bolometer was evaluated using light radiation on the membrane. We utilized bolometer “d” with a resistance ( $R_r$ ) of  $\approx 12.06$  k $\Omega$  and a  $G$  value of  $\approx 39.96$  nW K $^{-1}$  for this measurement. It was determined to be  $\approx 12.74$   $\mu$ V K $^{-1}$ , using Eq. (5). A light source was used for calibrating the bolometer’s response. We employed a blue light-emitting

diode (LED) with a wavelength of 490 nm as the radiation source. The LED power was quantified using an optical power meter at a distance between the light probe and the fiber of  $\approx 12$  mm. The lighting power density ( $D_L$ ) was then calculated by dividing the power meter detector area (0.79 cm $^2$ ). After positioning the fiber above the vacuum chamber, we illuminated the bolometer surface. The power induced in the bolometer ( $P_{IN}$ ) by radiation was calculated based on its area and the lighting power density (Fig. S3a and Table S1 in Supplementary Section 3). The lock-in amplifiers’ time constant was set to 1 ms, enabling the recording of thermal response and extraction of the  $\tau$  value using exponential curve fitting. Subsequently,  $V_B$ ,  $S$ , and  $B$  were set to 50, 500 mV, and 2000, respectively, resulting in a  $T_T$  of  $\approx 1.365$  V K $^{-1}$  and a power transformation coefficient ( $T_P$ ) of  $\approx 34.16$  mV nW $^{-1}$  (Fig. S3b in Supplementary Section 3).

### Evaluation of the AgNPs distribution on the bolometer membrane

The electrostatic adsorption of silver nanoparticles (AgNPs) onto bolometer membranes is influenced by the interplay of surface potentials initiated by the addition of diluted HCl. This process is significantly affected by the surface charge of Ti and Si materials, which are vital for interaction with citrate-stabilized AgNPs. These interactions are dependent on the isoelectric points of the natively oxidized surfaces (like TiO $_2$  and SiO $_2$ ) and the pH level of the AgNP dispersion. Effective surface interaction is expected in conditions where citrate remains deprotonated ( $pK_a > 3.1$ ), and the surface gains a positive charge through protonation. We used a scanning electron microscopy (SEM) type MIRA II SEM instrument (Tescan a.s.), setting its parameters, such as working distance and magnifications, to  $\approx 4.3$  mm and  $\times 7220$ , respectively, resulting in a field of view of 30  $\mu$ m. The SEM images were used to confirm the immobilization of AgNPs onto the microbolometer membranes at various pH levels by counting the number of particles using *Image J* software<sup>28</sup>. The number of AgNPs was calculated based on the total area occupied by them. Per the datasheet, the size of the AgNP was  $\approx 100$  nm. Thus the area of each particle was  $\approx 7850$  nm $^2$ , serving

**Table 1 | Thermal parameters and number of AgNPs on the membrane of each microbolometer used in the experiment**

Number	$R_r$ (k $\Omega$ )	$G$ (nW K $^{-1}$ )	$\tau$ (ms)	Number of AgNPs	Total $P$ (nW)	$P$ of AgNP (fW)
a	11.07	73.01	14.80	7049	1.2	170.2
b	11.37	55.63	15.78	8196	0.83	101.3
c	11.52	45.06	22.23	6576	1.23	187.0
d	12.06	39.96	22.99	7063	1.45	205.3
r1	10.15	41.02	20.34	0	\	\
r2	10.17	40.78	20.80	0	\	\

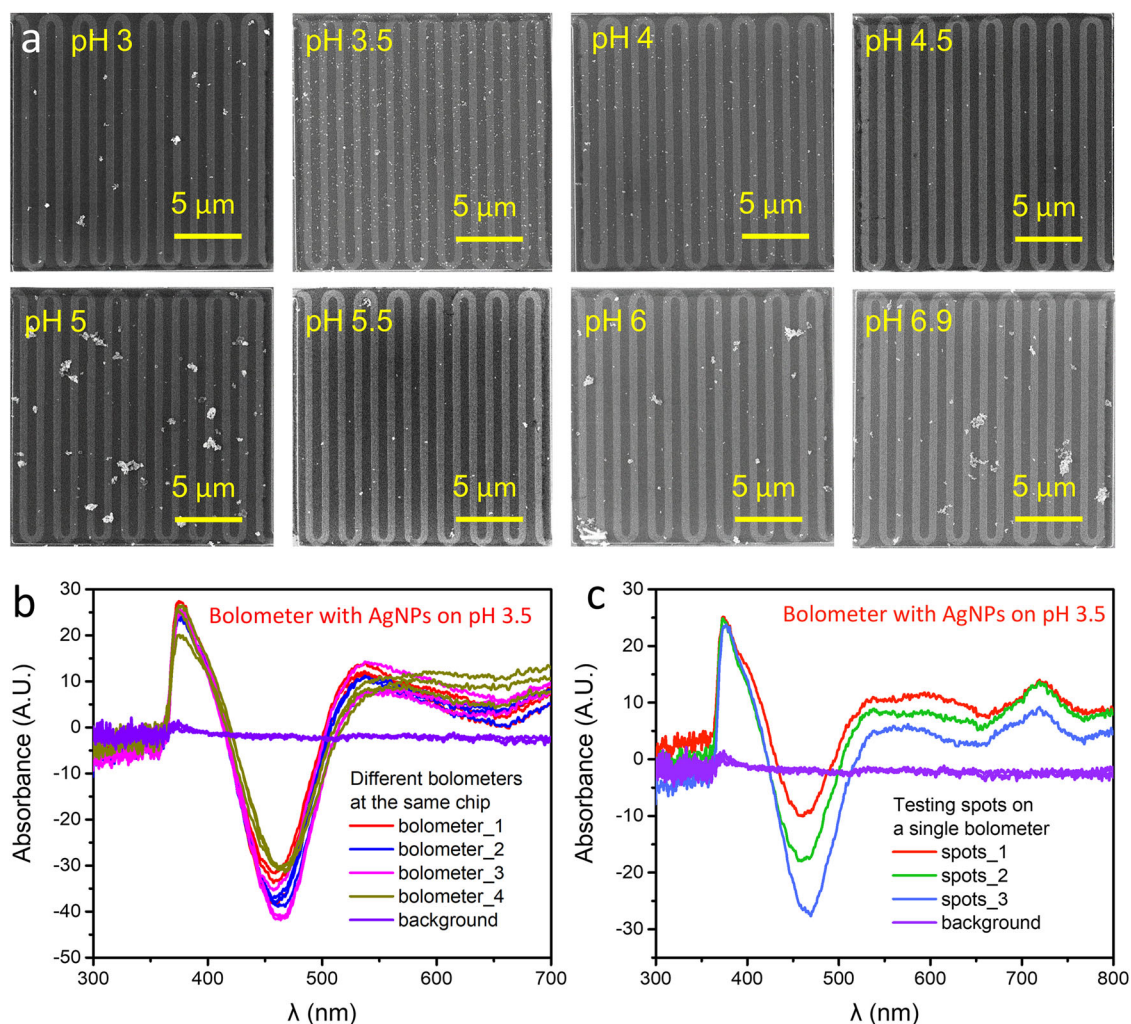


**Fig. 3 | Characterization of the deposited AgNPs on the bolometer membrane.** a SEM images of the bolometer membrane with adsorbed AgNPs at different pH values from 3.0 to 6.9 showing an optimized results at a pH of 3.5. b Measured relative light absorbance by scanning near-field optical microscopy (SNOM) at three

different spots at four bolometers having the AgNPs adsorbed at the membrane at pH of  $\approx 3.5$  as well as SNOM measurement at the membrane without AgNPs as background reference. c The SNOM measurement from a single device at three spots is marked in the SEM image of AgNPs in pH 3.5.

as the reference for the subsequent counting processes. Each SEM image was analyzed three times, and the average value of the number of AgNPs was obtained (Table 1).

The SEM images revealed that the AgNPs tend to aggregate below a pH of 3.5, a phenomenon likely due to the complete protonation of citrate molecules surrounding the nanoparticles. The concentration of  $\text{H}_3\text{O}^+$  ions in the surrounding environment crucially impacts the chemical equilibrium, causing changes in surface charge due to protonation or deprotonation. This change enhances the electrostatic interaction between the  $\text{SiO}_2$  on the bolometer surface and the AgNPs. We demonstrated the influence of the pH with AgNPs suspension to achieve the optimized spread of AgNPs across the membrane. Our focus was getting large area coverage without the formation of clusters. The best results were obtained using suspension with a pH of 3.5, as is shown in Fig. 3a.

The quantity of AgNPs adsorbed on the bolometer membrane increased as the pH of the colloidal suspension decreased, with aggregation observed below pH 3.5 and above 4.5. For light scanning measurements, we evaluated bolometer membranes with both high and low AgNP densities, prepared at pH 3.5 and 4.5, respectively. This approach allowed us to assess the signal from varying particle densities. Bolometers with aggregated AgNPs, especially those outside the ideal pH range, were excluded from further testing due to their adverse impact on the localized surface plasmon resonance (LSPR) effect. Our findings highlight the delicate balance

required in pH manipulation to optimize the adsorption of AgNPs onto bolometer membranes, underscoring the nuanced interplay between nanoparticle chemistry and surface physics. This understanding is crucial for advancing applications in high-precision sensors and nanoscale thermal imaging.

Optical absorbance measurements were performed using the Multi-View 4000 scanning near-field optical microscope (Nanonics Imaging Ltd.) in dark field observation mode. These measurements were conducted on three distinct spots, as shown in Fig. 3a, of a single bolometer, evaluated both with and without silver nanoparticles (AgNPs), to assess the uniformity of the measurements using an objective with 100 $\times$  magnification.

The absorbance spectrum revealed the immobilization of 100 nm AgNPs on the bolometer membrane at a pH of  $\approx 3.5$  measured at four different bolometers showed a peak absorbance at  $\approx 380$  nm (Fig. 3b). Moreover, a noticeable dip in absorbance was observed, reaching its lowest point at  $\approx 460$  nm. In contrast, the bolometer without AgNPs displayed a flat absorption curve, missing significant peaks, thus conclusively confirming the presence of AgNPs on the membrane. Details measured at the device with adsorption performed at a pH of 3.5 having an SEM image in (Fig. 3a) are shown in (Fig. 3c) and all measurements at 23 bolometers in Fig. S4 of Supplementary Section 4.

The variation in amplitude  $\approx 460$  nm could be attributed to impurities associated with the immobilization of AgNPs and the scattering effect,

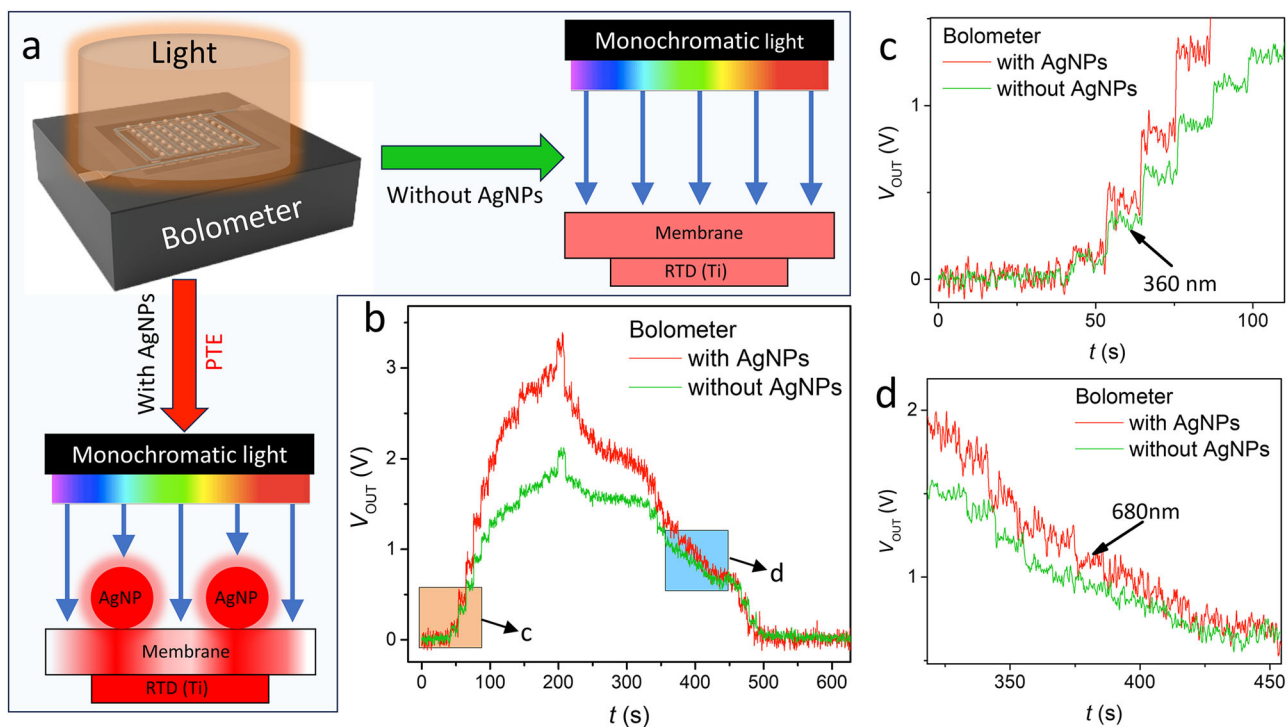


**Fig. 4 | Photothermal effect measurement of silver nanoparticles (AgNPs) using bolometer.** **a** Principal diagram of heat generation and transfer on bolometer membrane with and without AgNPs. **b** Response of the bolometer during light scanning in different  $\lambda$ . **c** The bolometers have identical responses when  $\lambda$  below

340 nm, and the difference increases with the changing of  $\lambda$ . **d** The response of monochromatic light back to the same level with  $\lambda$  of 680 nm for bolometer with and without AgNPs.

which may contribute to reflectance. This variation could also be due to changes in the roughness of the Si surface beneath the membrane following  $\text{XeF}_2$  etching<sup>29</sup>. It should be noted that the negative part of the spectra, although overlapping with the absorption maximum of AgNPs, does not hold significant meaning, as the device's construction did not allow for detailed analysis such as transmission spectra. The issue of the rough surface on the Si substrate beneath the membrane might be mitigated by prolonging the etching duration of Si, thereby distancing the substrate surface from the membrane. However, this method poses a substantial risk of under-etching the bolometer leads, potentially resulting in membrane collapse. A preferable strategy might involve adopting a different fabrication technology, which includes exposing the substrate from the backside to reduce scattered light and utilizing a silicon-on-insulator wafer as the substrate for bolometer fabrication. The actual SPR absorption maximum is not at  $\approx 380$  nm but rather higher, as later confirmed by power dissipation measurements. Manufacturer data indicates the maximum absorption range to be between 490 and 515 nm. Hence, the apparent discrepancy can likely be attributed to the aforementioned optical effects and the rough Si substrate beneath the bolometer membrane.

#### Calorimetry for localized surface plasmon resonance effect of AgNPs

The AgNPs utilized in our experiment exhibited a strong plasmonic resonance at a specific wavelength (SPR absorbance maxima) within the visible range. When illuminated with light that matched this SPR absorbance maximum, efficient photon-to-heat conversion occurred due to LSPR. This increased the temperature within the AgNPs, which was then immediately transferred to the bolometer membrane and measured by the temperature sensor (Fig. 4a). For reference, we also utilized a bolometer without AgNPs to respond directly to light. We investigated the bolometer's response to varying light wavelengths, particle counts, and sizes. The power detection limit of the employed bolometer was calculated to be  $\approx 26$  pW. We used a broadband light source from an Xe lamp with a nominal power of 100 W for

illumination and light detection. The light source was connected via a monochromator and spectrum analyzer, respectively (Fig. S5 in Supplementary Section 5).

The liquid core fiber was directly in contact with the optical window on the vacuum chamber, ensuring a constant distance between the fiber and the device. This maintained identical light conditions for different measurements. The  $\lambda$  of the light illuminating the bolometer membrane was varied from 300 to 800 nm in increments of 10 nm. Each wavelength was held for 10 s, allowing the bolometer to reach a stabilized state with a  $\tau$  of  $\approx 18$  ms. The filters inside the monochromator were adjusted based on the desired  $\lambda$  and duration. The response of the bolometer heating varied depending on the interrogating wavelength, so we used a bolometer without AgNPs as a benchmark to detect the effect of AgNPs' presence. We compared the measurements of the bolometer with and without AgNPs to observe the differences caused by the presence of nanoparticles (Fig. 4b). The response of the light scanning for  $\lambda$  below 350 nm was identical in both cases, with a similar increase observed for  $\lambda$  of 340 nm. However, the heat generation on the bolometer with AgNPs exhibited different behavior to the bolometer without AgNPs, from 350 to 680 nm (Fig. 4c and d). The additional heat generation was caused by enhanced light absorption when the AgNPs were presented at the surface.

#### Photothermal power output from a single AgNP

We performed measurements on various bolometers with different parameters and AgNPs, as listed in Table 1, to assess the response of the PTE. Four bolometers with varying distributions of AgNPs, along with two without AgNPs, were measured under identical conditions and settings. Each measurement was repeated four times (Fig. 5a). The bolometers without AgNPs exhibited good repeatability for  $\lambda$  ranging from  $\approx 300$  to  $\approx 780$  nm, with negligible differences observed for  $\lambda$  values exceeding  $\approx 500$  nm. The increase in response observed on the bolometer without AgNPs during  $\lambda$  scanning can be attributed to nonuniformity in monochromatic light intensity. Consequently, the average value obtained from

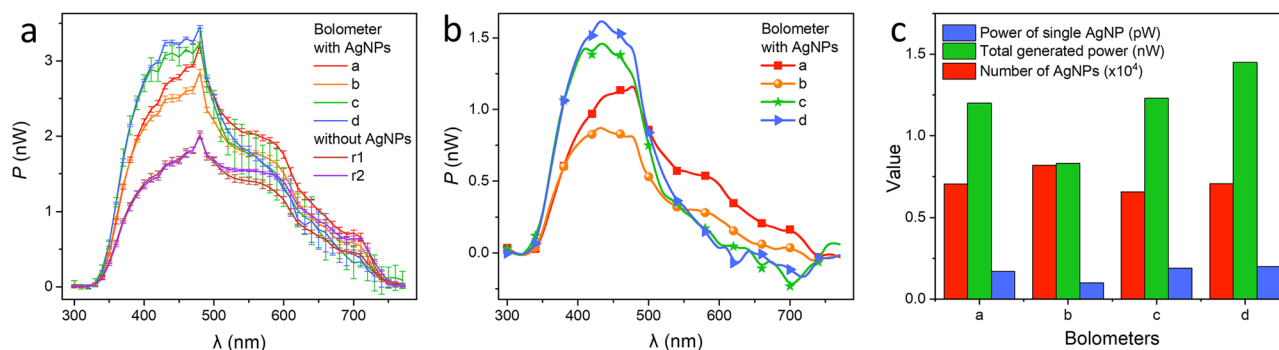


**Fig. 5 | Measurement results of heat generation from a single silver nanoparticle (AgNP).** **a** Response to the heat change of AgNPs on a bolometer using monochromatic light for wavelength scanning. **b** Subtracted power generation on different bolometers using the bolometer without AgNP as the baseline, showing AgNPs a

wide wavelength range sensitive to light. **c** Total power generated on the bolometer (green) and counted AgNPs on their surface (red), resulting in an average power generated from a single AgNP of (101.3–205.3) fW (data from four devices).

the measurements on bolometers without AgNPs was considered as a baseline for extracting heat generation by the PTE (Fig. 5b). Our results reveal that the absorption maxima of the AgNPs are between 400 and 500 nm. Results from all four bolometers are shown in Fig. 5c. We selected bolometer “d” for a detail description of the measurements. This device had a total 7063 AgNPs at its membrane and reached a maximum heat generation of  $\approx 1.45$  nW, corresponding to the heat generation by a single AgNP of  $\approx 205.3$  fW (Fig. 5c). The average AgNPs has a nominal diameter of 100 nm, corresponding to the area of  $7854$  nm<sup>2</sup>, which is  $7.85 \times 10^{-15}$  m<sup>2</sup>. Then, we can recalculate the heat generation at the unit of area of the AgNPs as  $\approx 22.9$  W m<sup>-2</sup>.

Our study revealed the interactions between the bolometer membrane and AgNPs. A central finding of our research is the precise determination of the power dissipated in a single AgNP, which was found to be between  $\approx 101.3$  and  $\approx 205.3$  fW. The enhanced PTE of AgNPs on the surface of a bolometer is based on the unique surface plasmon resonance properties of AgNPs. In addition to being influenced by the light source, it also significantly relates to the uniformity, density, and inter-particle spacing of the particles on the bolometer surface. Our process achieves the distribution of AgNPs on the bolometer surface by adjusting the pH value of AgNP colloidal dispersion. The adhesion behavior of AgNPs depends on both the bolometer membrane’s surface potential and the pH of the suspension containing the AgNPs. Effective adsorption of AgNPs was observed within the pH range of  $\approx 3.5$  to  $\approx 4.5$ . Outside this window, the nanoparticles tended to cluster. In terms of plasmonic properties, integrating AgNPs with micromachined bolometer membranes led to a marked increase in power dissipation when exposed to light near their resonance frequency. Our studies identified the peak of power dissipation to be  $\approx 460$  nm, even though the SNOM measurement showed that the resonance frequency is at a wavelength of  $\approx 480$  nm. However, even within the same batch of chips, there are differences in the distribution of AgNPs during self-assembly, leading to variations in photothermal power with the same light source. Therefore, representing the photothermal power of individual nanoparticles in terms of a range is more scientific than using a standard deviation. This significant achievement paves the way for a variety of practical applications and provides a clearer understanding of nanoparticle behavior at a single level.

The ability to measure and harness power from individual nanoparticles might revolutionize several fields<sup>30</sup>. Enhanced absorption and dissipation properties of AgNPs could significantly improve medical imaging tools, leading to clearer magnetic resonance imaging outputs. Moreover, the photon-to-heat conversion capability of AgNPs might play a crucial role in cancer treatments, offering a method to eliminate cancer cells while sparing healthy ones<sup>31,32</sup>. This phenomenon has paved the way for innovative developments, such as a new generation of polymerase chain reaction systems known as photonic PCR<sup>9,33</sup>. Outside the realm of

healthcare, AgNPs promise to transform environmental sensing with ultra-sensitive pollutant detectors and to advance spectroscopy across various sectors. Our study has brought to light the extraordinary attributes of AgNPs, especially when examined with an ultra-sensitive bolometer that possesses a power resolution of  $\approx 26$  pW. A pivotal discovery of our research is that a single AgNP can dissipate power with an amplitude between  $\approx 101.3$  and  $\approx 205.3$  fW, demonstrating the efficiency of its energy conversion from photon to heat. Conversely, the device enables the measurement of total dissipated power, facilitating the estimation of the number of AgNPs present on the bolometer surface. These insights provide a strong basis for further exploration into the physics of nanoparticle plasmons. The unique qualities of nanoparticles hold great promise for sparking innovations across a wide spectrum of fields, including imaging, spectroscopy, environmental monitoring, and medical treatments.

## Methods

### Bolometer fabrication

We initiated the lithography process by priming the substrate surface with hexamethyldisilazane (HMDS) vapor. We used a vacuum oven setting the temperature to  $150$  °C and performed the recommended sequence of pumping the oven to vacuum, purging with N<sub>2</sub>, and pumping again several times. Then we applied vapor of HMDS for 30 s, purged several times again and then vented.

We always used an i-line photoresist (PR) for lithography through the spin-coating process using  $\approx 4000$  RPM, achieving its recommended thickness of  $\approx 0.9$   $\mu$ m after pre-baking at  $\approx 110$  °C for  $\approx 60$  s. The PR was exposed by a 5:1 stepper and then post-baked using identical conditions as we used for pre-baking. The lithography process concluded with PR development using a tetramethylammonium hydroxide-based developer solution and the subsequent removal of any residual undeveloped PR using O<sub>2</sub> plasma for  $\approx 30$  s.

First, we formed the fiducial alignment marks in bare Si substrate by etching it after the lithography into a depth of  $\approx 0.1$   $\mu$ m using SF<sub>6</sub>/O<sub>2</sub>-based plasma. Then, we removed the PR and cleaned the wafers.

The first device fabrication step was the deposition of a  $\approx 0.25$   $\mu$ m layer of SiO<sub>2</sub> through a plasma-enhanced chemical vapor deposition process (PECVD) (Fig. 1b [i]) followed by sputter-deposition of a  $\approx 0.9$   $\mu$ m Al layer subsequently patterned to create bond pads and lead-outs (Fig. 1b [ii]). We sputter-deposited a  $\approx 0$  nm-thick Ti layer, which, after undergoing reactive ion etching, served as the temperature sensor on the bolometer membrane (Fig. 1b [iii]). A protective  $\approx 0.25$   $\mu$ m-thick SiO<sub>2</sub> layer covered the Ti sensor layer by PECVD. After patterning this layer to expose the bonding pads, we created Si substrate access holes for subsequent Si etching (Fig. 1b [iv]). XeF<sub>2</sub> vapor etching of the bolometer substrate isolated the bolometer membrane, minimizing heat losses to the Si substrate (Fig. 1b [v]). The process used here was the same as the one used before<sup>21,22,26</sup>.

## AgNPs deposition

Chemicals employed in the electrostatic deposition of AgNPs on the chips with bolometers encompassed an AgNP dispersion with a concentration of  $\approx 20 \mu\text{g ml}^{-1}$  and a nominal diameter of  $\approx 100 \text{ nm}$ , sourced from Sigma-Aldrich. This dispersion, stabilized using sodium citrate, presented a pH value near 6.9 and had a maximum extinction wavelength of  $\approx 480 \text{ nm}$ , as indicated by the material data sheet. Additional chemicals included HCl with a concentration of  $\approx 37\%$ , propane-2-ol (commonly known as isopropanol or IPA) with a purity of 99.98%, acetone with 99.5% purity, and deionized water (DI  $\text{H}_2\text{O}$ ). For pH adjustment purposes, the HCl was diluted with DI  $\text{H}_2\text{O}$  in a 1:100 ratio. The AgNP working solutions were prepared by mixing  $\approx 1.5 \text{ mL}$  of AgNP colloidal dispersion with the calculated quantity of diluted HCl. This ensured the adjustment of its pH to the specific values of 3, 3.5, 4, 4.5, 5, 5.5, 6, and 6.9.

The process of depositing AgNPs on the bolometer's surface involved an electrostatic adsorption technique using AgNP colloidal dispersion with different pH values. First, we cleaned the chips with bolometers using acetone to effectively remove organic residues and then cleaned them with IPA to eliminate any acetone traces. After being cleaned, the chips underwent a drying process using compressed  $\text{N}_2$ . Each cleaned chip with bolometers was then submerged into one of these AgNPs colloidal suspensions for a duration of  $\approx 2 \text{ h}$  (Fig. 1b [vi]). Post-immersion, the bolometer chips were cleaned with DI  $\text{H}_2\text{O}$  and then dried using compressed  $\text{N}_2$  (Fig. 1b [vii]). This methodological approach to fabrication was important in realizing a device of high performance, providing important insights into the photothermal dynamics related to AgNPs.

## Characterization of the bolometer

The RTD, made from Ti thin film, was utilized as the temperature sensing element<sup>27</sup>. We first evaluated its TCR. The bolometer chip was placed on a hotplate and its resistance was measured as a function of temperature using the four-point probe method. This resistance ( $R$ ) varied with temperature ( $\Delta T$ ) can be approximated by Eq. (1). Bolometer heat balance consists of dissipated Joule heat ( $P_j$ ), convection loss ( $P_{CV}$ ), radiation ( $P_R$ ), and conduction ( $P_{CD}$ ), achieved with Eq. (2):

$$P_j = \frac{V_B^2}{4R_t} = P_R + P_{CV} + P_{CD} \simeq P_{CD}. \quad (2)$$

In the vacuum testing environment,  $P_{CV}$  and  $P_R$  were negligible due to the calculated low  $G$  value of the bolometer device and the absence of a gaseous environment, respectively. The thermal conductance ( $G$ ), capacitance ( $H$ ), and temperature difference ( $\Delta T$ ) between the microbolometer membrane and the substrate chip define  $P_{CD}$ , as per Eq. (3):

$$P_{CD} = H \frac{d\Delta T}{dt} + G \cdot \Delta T. \quad (3)$$

The Wheatstone bridge output ( $\Delta V$ ) is achieved with Eq. (4):

$$\Delta V_L = \frac{10 \cdot B \cdot P \cdot \alpha \cdot V_B}{4 \cdot S \cdot G} = \frac{10 \cdot B \cdot \alpha \cdot V_B}{4 \cdot S} \Delta T = T_T \cdot \Delta T, \quad (4)$$

where  $B$  represents the amplifier gain,  $S$  is the lock-in amplifier sensitivity, and  $T_T$  is the transformation coefficient of temperature.  $T_T$  is then achieved with Eq. (5)<sup>22</sup>:

$$T_T = \frac{10 \cdot B \cdot \alpha \cdot V_B}{4 \cdot S}, \quad (5)$$

allowing for converting measured  $\Delta V_L$  into  $T$ .

## Data availability

Data are available upon request.

Received: 17 October 2023; Accepted: 22 April 2024;

Published online: 01 May 2024

## References

- Olson, J. et al. Optical characterization of single plasmonic nanoparticles. *Chem. Soc. Rev.* **44**, 40–57 (2015).
- Lim, W. Q. & Gao, Z. Plasmonic nanoparticles in biomedicine. *Nano Today* **11**, 168–188 (2016).
- Saha, K., Agasti, S. S., Kim, C., Li, X. & Rotello, V. M. Gold nanoparticles in chemical and biological sensing. *Chem. Rev.* **112**, 2739–2779 (2012).
- Dreaden, E. C., Alkilany, A. M., Huang, X., Murphy, C. J. & El-Sayed, M. A. The golden age: gold nanoparticles for biomedicine. *Chem. Soc. Rev.* **41**, 2740–2779 (2012).
- Huang, X. & El-Sayed, M. A. Plasmonic photo-thermal therapy (PPTT). *Alex. J. Med.* **47**, 1–9 (2011).
- Willets, K. A. & Van Duyne, R. P. Localized surface plasmon resonance spectroscopy and sensing. *Annu. Rev. Phys. Chem.* **58**, 267–297 (2007).
- Jain, P. K., Huang, X., El-Sayed, I. H. & El-Sayed, M. A. Review of some interesting surface plasmon resonance-enhanced properties of noble metal nanoparticles and their applications to biosystems. *Plasmonics* **2**, 107–118 (2007).
- Homola, J., Yee, S. S. & Gauglitz, G. Surface plasmon resonance sensors. *Sens. Actuators B: Chem.* **54**, 3–15 (1999).
- Kim, M., Lee, J. H. & Nam, J. M. Plasmonic photothermal nanoparticles for biomedical applications. *Adv. Sci.* **6**, 1900471 (2019).
- de Aberasturi, D. J., Serrano-Montes, A. B. & Liz-Marzán, L. M. Modern applications of plasmonic nanoparticles: from energy to health. *Adv. Opt. Mater.* **3**, 602–617 (2015).
- Zhou, C. et al. Activatable NIR-II plasmonic nanotheranostics for efficient photoacoustic imaging and photothermal cancer therapy. *Adv. Mater.* **33**, 2006532 (2021).
- Vines, J. B., Yoon, J.-H., Ryu, N.-E., Lim, D.-J. & Park, H. Gold nanoparticles for photothermal cancer therapy. *Front. Chem.* **7**, 167 (2019).
- Richards, P. L. Bolometers for infrared and millimeter waves. *J. Appl. Phys.* **76**, 1–24 (1994).
- Niesler, F. B. P., Gansel, J. K., Fischbach, S. & Wegener, M. Metamaterial metal-based bolometers. *Appl. Phys. Lett.* **100**, 203508 (2012).
- El Fatimy, A. et al. Epitaxial graphene quantum dots for high-performance terahertz bolometers. *Nat. Nanotechnol.* **11**, 335–338 (2016).
- Niklaus, F., Vieider, C. & Jakobsen, H. MEMS-based uncooled infrared bolometer arrays: a review. *Proceedings of SPIE, MEMS/MOEMS Technologies and Applications III*. 68360D-2 (2007).
- Huang, J., Wang, T., Zhu, P. & Xiao, J. Preparation, characterization, and thermal properties of the microencapsulation of a hydrated salt as phase change energy storage materials. *Thermochim. Acta* **557**, 1–6 (2013).
- Sarawade, A. A. & Charniya, N. N. Infrared Thermography and its Applications: A Review. *Proceedings of the International Conference on Communication and Electronics Systems (ICCES 2018)* 280–285 (IEEE).
- Husein, H. A. Thermal imaging for improving energy conservation behaviors: an infrared thermography survey for residential buildings. *ITJEMAST* **13**, 1–17 (2022).
- Kolibal, M. et al. Guided assembly of gold colloidal nanoparticles on silicon substrates prepatterned by charged particle beams. *ACS Nano* **6**, 10098–10106 (2012).
- Pekárek, J. et al. Self-compensating method for bolometer-based IR focal plane arrays. *Sens. Actuators A: Phys.* **265**, 40–46 (2017).
- Svatoš, V., Gablech, I., Ilic, B. R., Pekárek, J. & Neužil, P. In situ observation of carbon nanotube layer growth on microbolometers

- with substrates at ambient temperature. *J. Appl. Phys.* **123**, 114503 (2018).
23. Balram, K. C. et al. The nanolithography toolbox. *J. Res. Natl Inst. Stand. Technol.* **121**, 464 (2016).
  24. Zhang, H. et al. Nanolithography toolbox—simplifying the design complexity of microfluidic chips. *J. Vacuum Sci. Technol. B* **38**, 063002 (2020).
  25. Neuzil, P. & Mei, T. A method of suppressing self-heating signal of bolometers. *IEEE Sens. J.* **4**, 207–210 (2004).
  26. Svatoš, V., Gablech, I., Pekárek, J., Klempa, J. & Neuzil, P. Precise determination of thermal parameters of a microbolometer. *Infrared Phys. Technol.* **93**, 286–290 (2018).
  27. Neuzil, P. & Mei, T. Evaluation of thermal parameters of bolometer devices. *Appl. Phys. Lett.* **80**, 1838–1840 (2002).
  28. Schneider, C. A., Rasband, W. S. & Eliceiri, K. W. NIH Image to ImageJ: 25 years of image analysis. *Nat. Methods* **9**, 671–675 (2012).
  29. Liu, X., Zhu, H., Sabó, J., Lánský, Z. & Neuzil, P. Improvement of the signal to noise ratio for fluorescent imaging in microfluidic chips. *Sci. Rep.* **12**, 18911 (2022).
  30. Jiang, K., Smith, D. A. & Pinchuk, A. Size-dependent photothermal conversion efficiencies of plasmonically heated gold nanoparticles. *J. Phys. Chem. C* **117**, 27073–27080 (2013).
  31. Zhang, Y. et al. Tumor-targeting gene-photothermal synergistic therapies based on multifunctional polydopamine nanoparticles. *J. Chem. Eng.* **457**, 141315 (2023).
  32. Park, J. H. et al. Cooperative nanoparticles for tumor detection and photothermally triggered drug delivery. *Adv. Mater.* **22**, 880–885 (2010).
  33. You, M. et al. Ultrafast photonic PCR based on photothermal nanomaterials. *Trends Biotechnol.* **38**, 637–649 (2020).

### Author contributions

H.Z. prepared the optical setup (including a vacuum chamber), conducted optical measurements of the devices using modulated wavelength and processed data, and contributed to manuscript writing. E.G. prepared solutions with AgNPs and immobilized them on membranes, established optical spectra acquisition and data evaluation, and contributed to manuscript writing. I.G. is a co-inventor of the idea and was responsible for chips mounting into the socket and final etching using XeF<sub>2</sub>. He also contributed to the data evaluation, manuscript writing, and SEM image

capturing. P.N. devised the measurement and system properties evaluation and also contributed to measurement setup, data evaluation, and manuscript writing.

### Competing interests

The authors declare no competing interests.

### Additional information

**Supplementary information** The online version contains supplementary material available at <https://doi.org/10.1038/s43246-024-00509-0>.

**Correspondence** and requests for materials should be addressed to Imrich Gablech or Pavel Neuzil.

**Peer review information** *Communications Materials* thanks the anonymous reviewers for their contribution to the peer review of this work. Primary Handling Editor: Aldo Isidori. A peer review file is available.

**Reprints and permissions information** is available at <http://www.nature.com/reprints>

**Publisher's note** Springer Nature remains neutral with regard to jurisdictional claims in published maps and institutional affiliations.

**Open Access** This article is licensed under a Creative Commons Attribution 4.0 International License, which permits use, sharing, adaptation, distribution and reproduction in any medium or format, as long as you give appropriate credit to the original author(s) and the source, provide a link to the Creative Commons licence, and indicate if changes were made. The images or other third party material in this article are included in the article's Creative Commons licence, unless indicated otherwise in a credit line to the material. If material is not included in the article's Creative Commons licence and your intended use is not permitted by statutory regulation or exceeds the permitted use, you will need to obtain permission directly from the copyright holder. To view a copy of this licence, visit <http://creativecommons.org/licenses/by/4.0/>.

© The Author(s) 2024